Available online at www.sciencedirect.com
ScienceDirect
Journal of Nuclear Materials 367–370 (2007) 451–456
journal of nuclear materials
www.elsevier.com/locate/jnucmat

The effects of helium on irradiation damage in single crystal iron

Chaitanya S. Deo [b], Maria A. Okuniewski [a], Srinivasan G. Srivilliputhur [b], Stuart A. Maloy [b], Mike I. Baskes [b], Michael R. James [b], James F. Stubbins [a,*]

[a] *Department of Nuclear, Plasma and Radiological Engineering, University of Illinois at Urbana-Champaign, 214 Nuclear Engineering Laboratory, 103 South Goodwin Avenue, Urbana, IL 61801, USA*
[b] *Los Alamos National Laboratory, Los Alamos, NM 87545, USA*

Abstract

Fusion systems have a major issue with the relatively large amounts of helium (He) which are generated during the irradiation damage process. The effect of helium on the accumulation of defects and defect clusters and the influence of the resulting microstructure on physical and mechanical properties has been the focus of a large number of experimental and modeling studies over the past twenty years. The present work is part of an effort to quantify these effects in ways that were not possible in earlier studies. This is accomplished through systematic and coordinated computational modeling and experiments. The modeling approach employs both molecular dynamics (MD) and kinetic Monte Carlo (kMC) simulations to study the dynamic evolution of helium and defect clusters in bcc iron over relevant time scales. The kMC model follows the transport or evolution of the major defect entities in the material.

1. Introduction

During high-energy irradiation in a fusion environment, high-energy neutrons collide with atoms in the surrounding materials and induce $(n,\psi\alpha)$-reactions resulting in the formation of helium atoms. Reduced activation ferritic steels are attractive candidates for use as structural materials in fusion and accelerator driven reactors [1] as they show higher resistance to the degradation of material performance caused by neutron irradiation [2,3] and/or helium implantation [4] than other candidate materials.

First-wall materials in the fusion reactor (typically ferritic steels) contain a high concentration of helium atoms during and after irradiation [5,6]. These helium atoms have a strong tendency to precipitate into helium–vacancy clusters and bubbles, which are detrimental to the properties of metals and alloys. Mechanical properties such as tensile strength and fracture toughness [7,8] as well as embrittlement and fracture [9] are influenced by the presence of helium atoms. Thus, understanding helium behavior in metals is important in order to develop structural materials capable of operation in a high-energy proton irradiation environment.

The helium–vacancy cluster evolution under irradiation is governed by several mechanisms responsible for transport of helium atoms and vacancies in the crystal, such as the migrating helium interstitial,

* Corresponding author. Tel.: +1 217 333 6474; fax: +1 217 333 2906.
E-mail address: jstubbin@uiuc.edu (J.F. Stubbins).

0022-3115/$ - see front matter © 2007 Published by Elsevier B.V.
doi:10.1016/j.jnucmat.2007.03.117

migrating vacancy, thermally activated dissociation of helium from a vacancy and the jump of a He atom from one to another vacancy as a basic step in the vacancy mechanism [10]. A thermal mechanisms associated with displacements of helium atoms by self interstitials may be present at low temperatures [10]. It is generally believed [10,11] that diffusing helium rapidly clusters to form an evolving population of bubbles; these bubbles act as biased sinks for point defect fluxes.

In this paper, we will focus on a lattice based kinetic Monte Carlo (kMC) to simulate evolution of vacancies and helium in the post-cascade annealing stage during irradiation. Specifically we examine the modification of defect cluster evolution by the presence of helium during the post-cascade annealing stage in body centered cubic (bcc) iron. Input to the simulations may include the migration energies of the point defects, formation energies of the helium–vacancy clusters, dissociation energies of the point defects from the helium–vacancy clusters and initial concentrations and configurations of point defects and defect ratios. These energetic parameters can be obtained from MD simulations using empirical potentials or from first principles calculations. Similarly defect ratios and configurations can be obtained from the post-cascade data of large MD runs.

The only work along such lines for the Fe–He system has been performed by the following: Morishita, Wirth and co-workers [12,13] and Wirth and Bringa [14]. In one paper, Morishita and co-workers [13] performed molecular dynamics (MD) calculations to evaluate the thermal stability of helium–vacancy clusters in Fe using the Ackland Finnis–Sinclair potential, the Wilson–Johnson potential and the Ziegler–Biersack–Littmark–Beck potential for describing the interactions of Fe–Fe, Fe–He and He–He, respectively. In another paper, Morishita et al. [12] have looked at dissolution of helium–vacancy clusters as a function of temperature increase using the empirical potentials for the Fe–He system. Using the same potential system to describe Fe–He and a kinetic lattice Monte Carlo model, Wirth and Bringa [14] have simulated the motion of one single 2He–3Vac cluster at 1000 K.

The present kinetic Monte Carlo (kMC) simulations study the migration of point defects and the subsequent evolution of helium–vacancy bubbles using the same potential system. The intent of the paper is to understand the time and temperature dependence of the evolution of these small clusters during the post-cascade annealing stage. No additional sinks are included in the initial conditions as we wish to focus on the embryonic helium–vacancy cluster formation and the effect of temperature on that reaction. We are interested in the initial formation and evolution of small clusters (called embryonic bubbles in the paper) during post-cascade annealing stage of microstructural evolution following irradiation.

2. Simulation model and algorithm

In this paper, we will focus on a lattice based kinetic Monte Carlo (kMC) to simulate evolution of vacancies and helium in the post-cascade annealing stage during irradiation and the modification of defect evolution by the presence of helium in bcc iron. Fig. 1 shows the mechanisms by which the point defects migrate. The migration of the free (not clustered) helium and vacancies are illustrated in Fig. 1(a) and (b) respectively. The rates of migration of the point defect entities are calculated as

$$r^i_{\text{migration}} = v^i_{\text{migration}} \exp\left(-\frac{E^i_{\text{migration}}}{k_B T}\right), \tag{1}$$

where the superscript i refers to the helium and the vacancy point defect entities. The rate of migration of the point defect entity is $r^i_{\text{migration}}$, the attempt frequency is $v^i_{\text{migration}}$, the migration barrier is $E^i_{\text{migration}}$, while k_B and T are the Boltzmann constant and the temperature respectively. Dissociation of the helium and the vacancy from the cluster is described in Fig. 1(c) and (d) respectively. The rate of dissociation of a point defect entity (i = helium or vacancy) from a cluster into the bulk lattice is calculated as

$$r^i_{\text{dissociation}} = v^i_{\text{dissociation}} \exp\left(-\frac{E^i_{\text{dissociation}}}{k_B T}\right), \tag{2}$$

where $r^i_{\text{dissociation}}$ is the rate of dissociation, $v^i_{\text{dissocation}}$ is the attempt frequency, $E^i_{\text{dissociation}}$ is the energy of dissociation. The dissociation energy $E^i_{\text{dissociation}}$ of a point defect from a cluster is taken to be the sum of the energy to bind a point defect entity to the cluster and $E^i_{\text{migration}}$. Morishita et al. [13] have calculated the migration energies of helium and vacancies as well as the binding energies of some helium–vacancy clusters. These barriers are employed in these simulations. The attempt frequencies for the migration are taken to be of the order of the Debye frequency of iron (for vacancy migration) and that of helium (for helium migration). These parameters are used to calculate the rates of all the possible

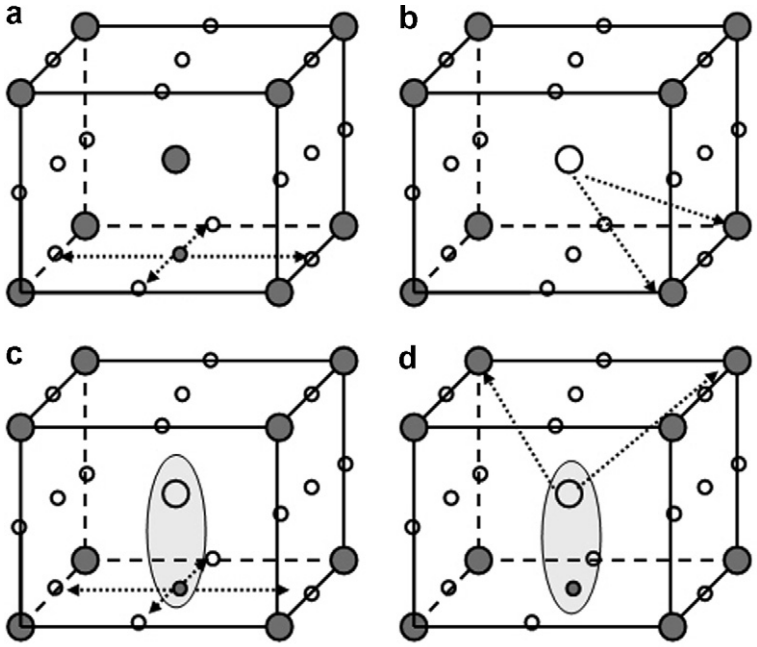

Fig. 1. The basic mechanisms of helium and vacancy activity in single crystal bcc iron. Large filled circles represent iron, large open circles represent vacancies, small filled circles represent helium atoms and small open circles represent the octahedral bcc sites. (a) Helium migration on the octahedral sublattice (b) Vacancy migration in bcc iron (c) Dissociation of helium from an embryonic bubble (d) dissociation of vacancy from an embryonic bubble.

events (Eqs. (1 and 2)) in the system and build the event catalog for the kMC simulation.

In the kMC event catalog, the transition probability of each event is proportional to the rate of event occurrence, calculated by the Eqs. (1) and (2). We follow the well established kMC simulation algorithm [15,16] which is a stochastic, atomic-scale method to simulate the time-evolution of defects and nano/microstructural evolution that focuses on individual defects and not on atomic vibrations.

At each kMC step, the system is monitored to identify a clustering event. When any two point defect entities are in a cluster the simulation creates a mapping between the entities and the cluster such that for each cluster there are at least two entities associated with the cluster. The event catalog is updated with the new rates of event occurrence and the transition probabilities for the next kMC event are calculated using Eqs. (1) and (2).

3. Defect evolution

We employ the above kMC model and algorithm to study helium and vacancy diffusion and clustering in the post-cascade annealing stage during irradiation. The interstitials diffuse by hopping to adjacent octahedral sites on the lattice while the vacancies diffuse by the vacancy mechanism on the substitutional bcc iron lattice. It is possible to introduce helium atoms and vacancy populations throughout the kMC simulation at rates appropriate to the irradiation environment. In the results presented here, we have 1000 helium atoms and vacancies distributed randomly in a $(200 \text{ unit cell})^3$ lattice. We have changed simulation box sizes from $(100 \text{ unit cell})^3$ to $(400 \text{ unit cell})^3$ and find that this affects the time scale of the evolution and not the qualitative mechanisms that operate in the simulation.

In Fig. 2, the number concentration of four defect species are plotted as a function of time, namely, free helium (squares), free vacancies (circles), helium–helium clusters (triangles) and helium–vacancy clusters ('x' symbol). The temperature of the system is maintained at $0.3T_m$, which for iron corresponds to a numerical value of 603 K.

The free helium concentration decreases far more rapidly than the free vacancy concentration. After the free helium concentration decreases to a negligible level, the free vacancy concentration decreases rapidly. The concentration of helium–helium clusters increases in the initial evolution phase, but decreases to a negligible amount at longer times.

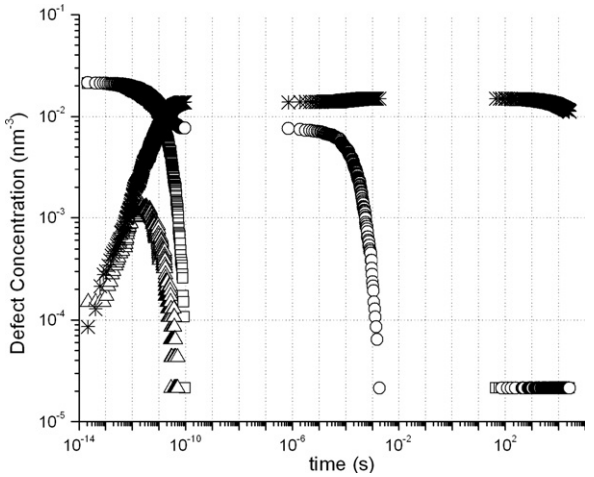

Fig. 2. Evolution of the number of defect species as a function of the simulation time. Free helium concentration (open squares), free vacancies (open circles), helium–helium clusters (open triangles) and helium–vacancy clusters ('x' symbol) are plotted. The simulation temperature is $0.3T_m$, where T_m is the melting point of iron.

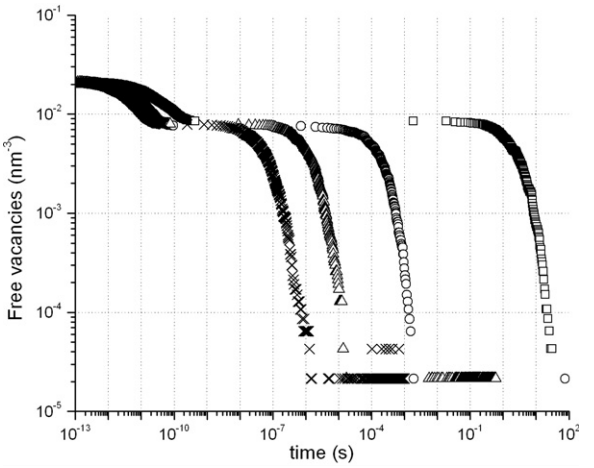

Fig. 3. Free vacancy concentration as a function of the simulation time at four temperatures: $T/T_m = 0.2$ (squares), 0.3 (triangles), 0.4 (circles), and 0.5 ('x' symbol), where T_m is the melting point of iron.

The concentration of helium–vacancy clusters shows three distinct stages of evolution. At lower times, the helium–vacancy cluster concentration increases, it remains fairly constant for several order of magnitude of time and then decreases at higher time scales. The initial increase in due to very small helium–vacancy clusters. Once the free helium is depleted, the size of the clusters grows by incorporating more vacancies. At longer time scales, point defects dissociate from smaller clusters and form larger clusters.

4. Effect of temperature on the free vacancy evolution

In Fig. 3, the number concentration of the free vacancy concentration is plotted as a function of time. Initial concentrations of point defect entities are the same as in the previous plot (Fig. 3). The evolution of the free vacancy concentration is plotted for four values of temperature, namely, $T/T_m = 0.2$ (squares), 0.3 (circles), 0.4 (triangles) and 0.5 ('x' symbol).

The free vacancy concentration decreases from its initial value to nearly negligible concentration at longer times. At long times all the vacancies are incorporated in defect clusters or bubbles. There are two regions of free vacancy evolution which are separated by several orders of magnitude of time. Initially, the decrease in free vacancy concentration corresponds to the migration of the helium atoms and their clustering with vacancies. At longer times, all the helium is incorporated in embryonic clusters and the vacancies migrate leading to a decrease in their concentration. As the temperature increases, the free vacancy concentration evolves faster as is expected from a thermally activated process (Eq. (1)).

5. Effect of temperature on the cluster evolution

In Fig. 4, we plot the evolution of helium vacancy clusters (Fig. 4a) and helium–helium clusters (Fig. 4b) as a function of time for three temperatures, namely, $T/T_m = 0.2$ (squares), 0.3 (circles), and 0.5 (triangles). Initial concentrations of point defect entities are the same as in the previous plot (Fig. 3).

As noted before, the helium–vacancy clusters evolution shows three distinct stages. The temperature affects the times scales of these regimes, especially last two stages: the growth of embryonic bubbles due to vacancy migration and the coalescence of bubbles due to dissociation of point defects from smaller bubbles.

The helium–helium clusters increase in time at lower times and decrease to a negligible value at longer times. With increasing temperatures, the maximum number of helium–helium clusters formed also decreases. Dissociation of helium from these clusters occurs more frequently at higher

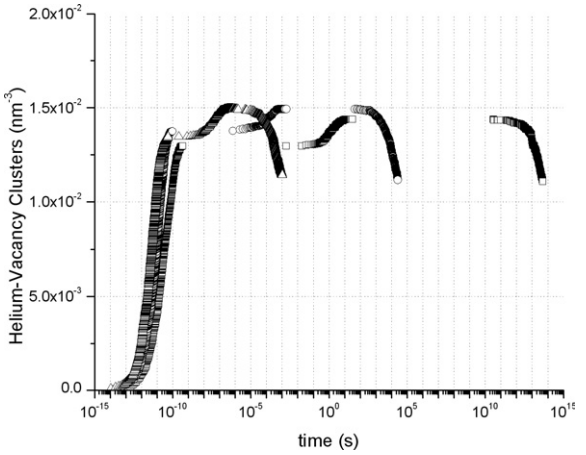

Fig. 4a. Helium–vacancy cluster concentration as a function of the simulation time for three temperatures: $T/T_m = 0.2$ (squares), 0.3 (circles), and 0.5 (triangles), where T_m is the melting point of iron.

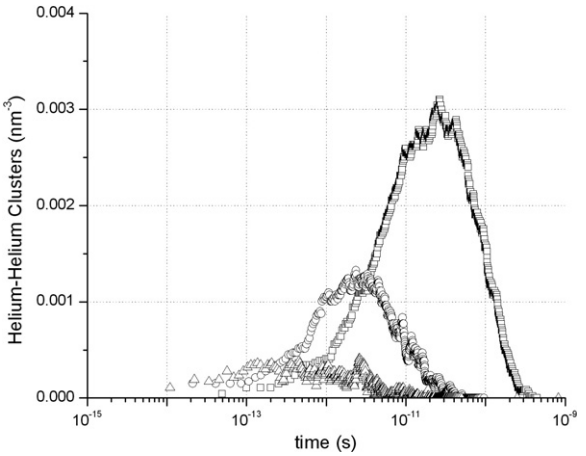

Fig. 4b. Helium–helium cluster concentration as a function of the simulation time for temperatures: $T/T_m = 0.2$ (squares), 0.3 (circles), and 0.5 (triangles), where T_m is the melting point of iron.

temperatures. The binding energy of helium from helium–helium clusters is much smaller (0.3 eV) than the binding energy of helium to a vacancy (2.0 eV) as calculated by Morishita et al. [13], leading to the dissolution of helium–helium clusters and the temperature effects observed in Fig. 4b.

6. Discussion and summary

We have employed the kMC simulations to investigate the time-evolution of the point defects leading to defect clustering and bubble formation. As mentioned earlier, previous work along such lines for the Fe–He system has been performed by Morishita and co-workers [12,13] and Wirth and Bringa [14]. Morishita et al. [13] performed molecular dynamics calculations to evaluate the thermal stability of helium–vacancy clusters and in reference [12] have employed kMC simulations to evaluate dissolution of helium–vacancy clusters as a function of temperature increase. Wirth and Bringa [14] have simulated the motion of one single 2He–3Vac cluster at 1000 K. In that paper, two interstitial helium atoms were placed in close proximity to a trivacancy cluster. The two helium atoms were found to cluster with the vacancy cluster with ~100 ps.

We are investigating the initial formation of small clusters (embryonic bubbles in the text). The intent of the paper is to understand the time and temperature dependence of the evolution of these small clusters during the initial annealing stage following a cascade. The simulations are performed over much longer time scales than previous work and investigate the initial formation of helium–vacancy bubbles given a concentration of randomly distributed helium and vacancies.

We have repeated these simulations for a wide variety of the initial configurations by changing the initial simulation size and maintaining the same number of defects in that simulation cell. We find that the qualitative evolution of the system does not change with varying concentrations. The only quantitative effect is the time scale of the simulation, i.e., systems with smaller simulation sizes (higher concentrations) evolve faster than systems with larger simulation sizes.

No sinks are included in the simulations presented in this paper apart from vacancies and embryonic bubbles themselves as sinks for migrating point defects. We are interested in the initial formation of small clusters immediately following the formation of a cascade and the effect of temperature on this formation; hence sinks have not been introduced. The presence of sinks will serve to reduce the number concentration of the embryonic helium–vacancy bubbles. Thus, the results presented here are an upper bound on the number of initial clusters (embryonic bubbles) formed during post-cascade annealing conditions. Future work will clarify the mobility of vacancy–He cluster complexes and extend the simulation durations to predict He bubble nucleation as well as include sinks of varied strengths to simulation the nucleation and growth of gas stabilized bubbles during post-cascade microstructural evolution.

References

[1] N. Hashimoto, S.J. Zinkle, et al., in: Materials Research Society Symposium – Proceedings Microstructural Processes in Irradiated Materials-2000, November 27–29, 2000; Boston, MA, United States, 2001. 650, p. R1.10.1.
[2] A. Kohyama, A. Hishinuma, et al., J. Nucl. Mater. 233/237A (1996) 138.
[3] A. Kimura, M. Narui, et al., J. Nucl. Mater. 263 (1998) 1340.
[4] H. Ullmaier, MRS Bull. 22 (4) (1997) 14.
[5] F. Garner, B. Oliver, et al., J. Nucl. Mater. 296 (2001) 66.
[6] B.M. Oliver, M.R. James, et al., J. Nucl. Mater. 307 (2002) 1471.
[7] S. Maloy, M. James, et al., J. Nucl. Mater. 318 (2003) 283.
[8] S.A. Maloy, M.R. James, et al., in: 3rd Workshop on Utilisation and Reliability of High Power Proton Accelerators, OECD, 2003, p. 105.
[9] T.R. Armstrong, P.J. Goodhew, Radiat. Eff. 77 (1/2) (1983) 35.
[10] H. Trinkaus, B.N. Singh, J. Nucl. Mater. 323(2/3) 229.
[11] M. Baskes, R. Fastenau, et al., J. Nucl. Mater. 102 (3) (1981) 235.
[12] K. Morishita, R. Sugano, B.D. Wirth, J. Nucl. Mater. 323 (2/3) (2003) 243.
[13] K. Morishita, R. Sugano, et al., Nucl. Instrum. and Meth. B 202 (2003) 76.
[14] B.D. Wirth, E.M. Bringa, Phys. Scr. T108 (2004) 80.
[15] D.T. Gillespie, J. Phys. Chem. 81 (25) (1977) 2340.
[16] A.B. Bortz, M.H. Kalos, J.L. Lebowitz, J. Comput. Phys. 17 (1) (1975) 10.